$-\Delta G^{\circ}_{AB}$ and pH Dependence of the Electron Transfer from $P^+Q_A^-Q_B$ to $P^+Q_AQ_B^-$ in *Rhodobacter sphaeroides* Reaction Centers†

Jiali Li,‖ Eiji Takahashi,‡ and M. R. Gunner*

Department of Physics, City College of New York, 138th Street and Convent Avenue, New York, New York 10031, and Department of Plant Biology, University of Illinois, 1201 West Gregory Drive, Urbana, Illinois 61801

Received November 9, 1999; Revised Manuscript Received March 15, 2000

ABSTRACT: The electron transfer from the reduced primary quinone (Q_A^-) to the secondary quinone (Q_B) can occur in two phases with a well-characterized 100 μs component (τ_2) and a faster process occurring in less than 10 μs (τ_1). The fast reaction is clearly seen when the native ubiquinone-10 at Q_A is replaced with naphthoquinones. The dependence of τ_1 on the free-energy difference between the $P^+Q_A^-Q_B$ and $P^+Q_AQ_B^-$ states ($-\Delta G^{\circ}_{AB}$) and on the pH was measured using naphthoquinones with different electrochemical midpoint potentials as Q_A in *Rhodobacter sphaeroides* reaction centers (RCs) and in RCs where $-\Delta G^{\circ}_{AB}$ is changed by mutation of M265 in the Q_A site from Ile to Thr (M265IT). Q_B was ubiquinone (UQ_B) in all cases. Electron transfer was measured by using the absorption differences of the naphthosemiquinone at Q_A and the ubisemiquinone at Q_B between 390 and 500 nm. As $-\Delta G^{\circ}_{AB}$ was changed from −90 to −250 meV τ_1 decreased from 29 to 0.2 μs. The free-energy dependence of τ_1 provides a reorganization energy of 850 ± 100 meV for the electron transfer from Q_A^- to Q_B. The slower reaction at τ_2 is free-energy independent, so processes other than electron transfer determine the observed rate. The fraction of the reaction at τ_1 increases with increasing driving force and is 100% of the reaction when $-\Delta G^{\circ}_{AB}$ is ≈100 meV more favorable than in the native RCs with ubiquinone as Q_A. The fast phase, τ_1, is pH independent from pH 6 to 11 while τ_2 slows above pH 9. As the Q_A isoprene tail length is increased from 2 to 10 isoprene units the fraction at τ_1 decreases. However, τ_1, τ_2, and the fraction of the reaction in each phase are independent of the tail length of UQ_B.

The photosynthetic reaction center (RC) of purple nonsulfur bacteria is the protein−cofactor complex that performs the initial steps in the conversion of light energy to chemical energy by a series of electron-transfer reactions (Figure 1) (*1*−*4*). In isolated RCs, following absorption of a photon by a dimer of bacteriochlorophylls (P),[1] an electron on P is transferred to the tightly bound primary quinone (Q_A) within 200 ps (Figure 1). The subsequent electron transfer from Q_A^- to the secondary quinone (Q_B) occurs within 3−200 μs yielding $P^+Q_B^-$ at $k_{AB}^{(1)}$ (*5*−*10*). In chromatophores the semiquinone Q_B^- is protonated below pH 6 (*11*), but in isolated RCs neither Q_A^- nor Q_B^- binds a proton (*12, 13*). With an electron donor to reduce P^+, a second photon initiates another turnover in which Q_B^- becomes doubly reduced and protonated at $k_{AB}^{(2)}$ (*14*). It then dissociates from the protein as the dihydroquinone, QH_2. In *Rhodobacter sphaeroides* RCs Q_A and Q_B are both ubiquinones that are modified by the protein to play their different roles in the reaction cycle.

The early, fast electron-transfer reactions forming $P^+Q_A^-$ show little temperature or pH dependence indicating that these can occur in a relatively rigid protein. In contrast, the electron transfer from Q_A^- to Q_B has significant temperature and pH dependence (*8, 15, 16*). An electron transfer from Q_A^- to Q_B that occurs at ≈100 μs (22 °C, pH 8) has been studied intensively. This reaction is pH independent from pH 6 to 9 and is faster at lower and slower at higher pH. Thus, in the intermediate pH range there is little proton uptake from solution on electron transfer from Q_A^- to Q_B (*17*−*21*). The rate is independent of the free-energy differ-

† The Department of Agriculture CSREES 1999-01256 and National Science Foundation MCB-9629047 provided financial support. NIH RR03060 provided maintenance of central facilities.

* Corresponding author: Marilyn R. Gunner, Department of Physics, Rm. J419, City College of New York, 138th St. and Convent Ave., New York, NY 10031. Phone: 212-650-5557. Fax: 212-650-6940. E-mail: gunner@sci.ccny.cuny.edu.

‡ University of Illinois.

‖ Current address: Physics Department, Harvard University, 17 Oxford St., Jefferson Labs, Cambridge, MA 02138

[1] Abbreviations: P is the bacteriochlorophyll dimer which is the primary electron donor in the reaction center protein; H_L is the bacteriopheophytin near Q_A on the L branch of the protein while H_M is near Q_B on the M branch; UQ_1 is 2,3-dimethoxy-5-methyl-6-[3-methyl-2-butenyl]-1,4-benzoquinone; UQ_{10} (Ubiquinone-10) is 2,3-dimethoxy-5-methyl-6-decaisoprenyl-1,4-benzoquinone; MQ (vitamin K_1) is 2-methyl-3-phytyl-1,4-naphthoquinone; NQ_2 (menaquinone-2) is 2-methyl-3-ethylisoprenyl-1,4-naphthoquinone; NQ_4 (menaquinone-4) is 2-methyl-3-tetraisoprenyl-1,4-naphthoquinone; NQ_{10} (menaquinone-10) is 2-methyl-3-decaisoprenyl-1,4-naphthoquinone; Me_2NQ is 2,3-dimethyl-1,4-naphthoquinone; Me_3NQ is 2,3,5-trimethyl-1,4-naphthoquinone; Me_4NQ is 2,3,6,7-tetramethyl-1,4-naphthoquinone; P^+Q^- difference spectrum is the absorption of P^+Q^- minus that of PQ; Q^- spectrum is the semiquinone minus quinone spectrum; $-\Delta G^{\circ}_{AB}$ is the free-energy difference between $Q_A^-Q_B$ and $Q_AQ_B^-$ states; $k_{AB}^{(1)}$ is the rate of the electron transfer from $P^+Q_A^-Q_B$ to form $P^+Q_AQ_B^-$ including all phases and all associated processes; τ_1, τ_2, and τ_3 are the lifetimes with associated amplitudes A_1, A_2, and A_3 of the fast (<10 μs), intermediate (≈100 μs), and slow (>500 μs) phases, respectively, of the ($P^+Q_A^-Q_B \rightarrow P^+Q_AQ_B^-$) electron transfer.

10.1021/bi992591f CCC: $19.00
Published on Web 05/31/2000

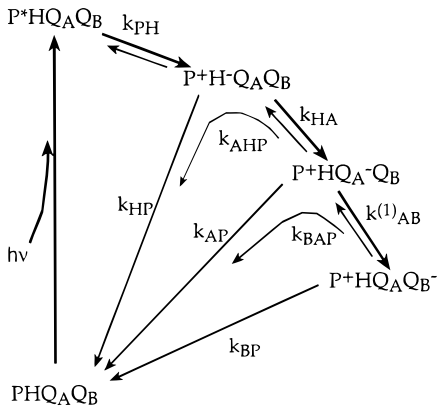

FIGURE 1: Electron-transfer pathways in bacterial RCs. First, an electron on the bacteriochlorophyll dimer (P) is promoted to the excited singlet state (P*) by absorption of a photon. Initial charge separation to the active bacteriopheophytin (H) 15 Å away occurs in 4 ps with a $-\Delta G^{\circ}_{PH} \approx 160$ meV forming P^+H^-. In 200 ps the electron moves to the tightly bound primary quinone, Q_A, 10.1 Å from H. The reaction $-\Delta G^{\circ}_{HA}$ is ≈670 meV. The subsequent electron transfer from Q_A to the secondary quinone, Q_B, 14.5 Å from Q_A with $-\Delta G^{\circ}_{AB} \approx 60$ meV, has been measured to occur within 3−200 μs yielding $P^+Q_B^-$. If there is no exogenous donor to reduce P^+, the electron on the acceptor quinone will return to P^+ in a charge-recombining back-reaction. The back-reactions from Q_A or Q_B to P^+ (22.5 and 23.4 Å, respectively) each have two pathways (eqs 1 and 2), with rates k_{BP} or k_{AP} where the electron tunnels directly to P^+, and k_{BAP} or k_{BHP} where the electron goes to P^+ via a higher energy state. The intermediate state is $P^+Q_A^-Q_B$ for $P^+Q_B^-$ and $P^+H^-Q_A$ for $P^+Q_A^-$. The forward electron-transfer reactions are highlighted by the thicker arrows. In the figure the redox states of all cofactors are explicitly noted. The more compact nomenclature used in the figure legend which omits the neutral sites (e.g., $P^+Q_B^-$ for $P^+HQ_AQ_B^-$) is used in the text.

ence between $Q_A^-Q_B$ and $Q_AQ_B^-$ ($-\Delta G^{\circ}_{AB}$) (*7*). Thus, the electron transfer itself does not control the ≈100 μs phase of this reaction. Some other process such as motion of the protein or cofactors, or proton transfer, determines the rate. The enthalpy of the reaction is ≈3.5 kcal/mol (*8, 10*), although earlier measurements had provided larger values (*15*). Thus, the rate-determining process has a modest enthalpy barrier.

A faster phase of the electron transfer from Q_A^- to Q_B has been observed in *Rb. sphaeroides* RCs in chromatophores (*8, 9*). At room temperature, 60% of the reaction occurs at 3.5 μs and 40% at 80 μs. In isolated RCs when 2-methyl-3-phytyl-1,4-naphthoquinone (MQ) replaces ubiquinone-10 (UQ_{10}) in the Q_A site (designated here as MQ_A) and UQ_{10} is retained as Q_B (UQ_B) spectral changes are seen with lifetimes τ_1 of 3 ± 0.9 μs, τ_2 of 80 ± 20 μs, and τ_3 of 0.4 ± 0.2 ms (22 °C, pH 8) (*10*). Since the spectrum of menasemiquinone (MQ^- λ_{max} at 400 nm) is different from that of ubisemiquinone (UQ^-, λ_{max} at 450 nm) (*22*−*24*), quinone substitution provides a direct monitor of the transfer of the electron from MQ_A^- to UQ_B. The time-resolved spectral changes in the MQ_AUQ_B RCs of the semiquinones in the near-UV and the electrochromic response of the bacteriopheophytin and bacteriochlorophylls in the near-IR were determined. These show that the changes at τ_1 are mostly due to electron transfer, while electron transfer and charge compensation are mixed in τ_2, and little electron transfer occurs at τ_3 (*10*). In RCs with MQ_AUQ_B 60% of the electron transfer occurs at τ_1 and 40% at τ_2. However, only the ≈100 μs phase is seen in isolated RCs with UQ_A and UQ_B.

The work presented here compares and contrasts the driving force ($-\Delta G^{\circ}_{AB}$) and pH dependence of the faster reaction (τ_1) and the previously studied ≈100 μs process (τ_2). The reaction free energy was changed by substituting quinones with different redox potentials for ubiquinone at the Q_A site in *Rb. sphaeroides* R-26 RCs and by the use of the Q_A site mutant M265IT (*25, 26*). Dependence of the rate on $-\Delta G^{\circ}_{AB}$ provides evidence that τ_1 monitors the electron transfer itself rather than some conformational change as found with the free-energy-independent ≈100 μs phase of the reaction (*7*). In addition, the fraction of the Q_A^- to Q_B electron transfer occurring in the two phases changes with $-\Delta G^{\circ}_{AB}$. This begins to establish when the reaction can occur rapidly instead of being restricted to the gated ≈100 μs process.

MATERIALS AND METHODS

Protein Isolation. Rb. sphaeroides RCs were isolated by standard procedures using lauryldimethylamine-*N*-oxide (LDAO, Calbiochem) detergent extraction followed by purification using ammonium sulfate and DEAE chromatography (*27*). The ubiquinones at the Q_A and Q_B sites were removed with orthophenanthroline using the method of Okamura (*28*), with minor modifications (*29*). This method typically yields RCs with no UQ_B and ≈5% UQ_A. The RC concentration was determined at 802 or 865 nm using the extinction coefficients $\epsilon_{802} = 0.288$ $\mu M^{-1}cm^{-1}$ or $\epsilon_{865} = 0.135$ $\mu M^{-1}cm^{-1}$, respectively.

M265IT RCs. RCs with isoleucine at M265 replaced by threonine (M265IT) were prepared in a carotonoid containing *Rb. sphaeroides* Ga strain (*25, 26*). The mutation has been shown to lower the in situ electrochemical midpoint of Q_A^-/Q_A by about 120 mV, thereby increasing the free energy of electron transfer from Q_A^- to Q_B ($-\Delta G^{\circ}_{AB}$) by 120 meV.

Quinones Used for Reconstitution of Q_A Function. The quinone MQ (2-methyl-3-phytyl-1,4-naphthoquinone, vitamin K_1) was purchased from Fluka; UQ_0, UQ_1, UQ_2, UQ_4, and UQ_{10} were purchased from Sigma; and Me_2NQ, NQ_2, NQ_4, NQ_{10}, and Me_4NQ were gifts from C. C. Moser and P. L. Dutton. Me_3NQ and some Me_4NQ were gifts from M. S. Graige and M. Y. Okamura. See Table 1 for the full name of each compound. The Me_3NQ and Me_4NQ were synthesized by Paul L. Williams and Malcolm Bruce at the University of Manchester.

The long-tailed quinones are insoluble in water but become soluble when detergent is added. However, detergent weakens the affinity of quinone for the binding sites. Dissolving the quinone in Triton X-100 permits effective and reproducible reconstitution of long-tailed quinones (*30*). Quinones with tails shorter than four isoprene units were dissolved in ethanol.

Optical Measurements. Transient absorption kinetics were obtained by using a continuous measuring beam, and the resulting data were analyzed as described previously (*10*). To improve the signal-to-noise ratio in the measurement of lifetimes less than 5 μs, a 10-μs (full width at half-maximum) xenon flash provided a more intense brief measuring light. A National Instruments Labview program was used to run each cycle of measurement. This program fired the Con-

Table 1 [a]

Q_A	k_{AP}^{obs} (s^{-1})	Q_B	k_{BP}^{obs} (s^{-1})	$-\Delta G_{AB}$ (meV)	$-\Delta G_{AB}$ determined	k_1 ($\times 10^6\ s^{-1}$)	$\pm$[b]	k_2 (s^{-1})	fraction at A_1
				R-26					
UQ_{10}	9.3 ± 0.2	UQ_{10}	0.85	60	A	–	–	15385	<0.1
MQ	13.6 ± 0.6	UQ_1	0.81	72	A	0.098	0.34	9741	0.30
MQ	13.6 ± 0.6	UQ_2	0.77	73	A	0.036	0.16	11420	0.45
MQ	13.6 ± 0.6	UQ_4	0.47	87	A	0.094	0.12	9118	0.46
MQ	13.6 ± 0.6	UQ_{10}	0.38	93	A	0.286	0.28	12500	0.60
NQ_2	15.5 ± 0.8	UQ_{10}	0.50	86	A	0.114	0.10	5000	0.45
NQ_4	15.0 ± 1.0	UQ_{10}	0.45	94	A	0.159	0.12	8800	0.40
NQ_{10}	15.0 ± 0.9	UQ_{10}	0.40	94	A	0.294	0.40	2400	0.28
Me_2NQ	8.2 ± 0.1	UQ_1	0.88	60	B1	0.103	0.43	10153	0.30
Me_3NQ	15.5 ± 0.9	UQ_1	0.16	130	B1	2.3	0.30	5026	0.75
Me_4NQ	25.0 ± 0.2	UQ_1	0.19	160	B2	1.7	0.40	nd	1.00
				M265IT					
UQ_{10}	25	UQ_{10}	0.16	160	B2	–	–	nd	<0.1
MQ	38 ± 3	UQ_{10}	0.10	213	B2	3.3	0.36	9490	nd
Me_2NQ	29 ± 1	UQ_1	0.37	180	B2	4.96	0.19	9280	nd
Me_3NQ	400 ± 10	UQ_1	0.48	250	B2	1.3	0.50	5723	nd

[a] UQ_1 is 2,3-dimethoxy-5-methyl-6-[3-methyl-2-butenyl]-1,4-benzoquinone; UQ_{10} (ubiquinone-10) is 2,3-dimethoxy-5-methyl-6-decaisoprenyl-1,4-benzoquinone; MQ (vitamin K_1) is 2-methyl-3-phytyl-1,4-naphthoquinone; NQ_2 (menaquinone-2) is 2-methyl-3-ethylisoprenyl-1,4-naphthoquinone; NQ_4 (menaquinone-4) is 2-methyl-3-tetraisoprenyl-1,4-naphthoquinone; NQ_{10} (menaquinone-10) is 2-methyl-3-decaisoprenyl-1,4-naphthoquinone; Me_2NQ is 2,3-dimethyl-1,4-naphthoquinone; Me_3NQ is 2,3,5-trimethyl-1,4-naphthoquinone; Me_4NQ is 2,3,6,7-tetramethy-1,4-naphthoquinone. The percentage error for k_1 was determined from the standard deviation of the kinetic analysis. k_{AP} and k_{BP} are defined in Figure 1. $-\Delta G^\circ_{AB}$ was determined as described in the Methods section: (A) from the back-reaction at k_{BAP}; (B1) using the E_m of Q_A determined by delayed fluorescence; (B2) using the E_m of Q_A determined from k_{AHP}. [b]The percentage uncertainty in the given rate.

tinuum Laser flash lamps at 10 Hz and triggered a Stanford timing box (Stanford Research Systems Inc. DG535) every 2 min. The Stanford timing box triggered the xenon measuring flash and the laser Q switch. A background signal was collected (I_b) with both xenon flash measuring light and laser actinic flash blocked from the sample. Then a reference signal (I_r) was collected with the xenon flash through the sample but with the laser excitation blocked ($I_o = I_r - I_b$). Finally, measurements with both laser and xenon flash through the sample provided I_s; then, $I_x = I_s - I_b$. Measurements for I_b, I_r, and I_s were averaged 100 times. This diminished the effects of jitter in the synchronization of the laser (± 1 ns) and the xenon flash (200 ns). The jitter of the trigger to delay the laser Q-switch after the initiation of the xenon flash is 50 ps. After averaging, I_o for the xenon flash was found to be reproducible despite the jitter in the initiation of this pulse. The absorption change due to the reaction was then calculated using $\Delta A(t) = \log(I_o(t)/I_x(t))$.

Estimation of $-\Delta G^\circ_{AB}$ for the Reaction $P^+XQ_A^-UQ_B$ to $P^+XQ_AUQ_B^-$. It is necessary to determine the free energy of the electron transfer from each substituted Q_A (XQ_A) to the ubiquinone at Q_B. Two methods are used: (A) determine $-\Delta G^\circ_{AB}$ by the back-reaction from Q_B^- via Q_A^- at k_{BAP}; (B) determine the in situ redox potentials, $E_m(Q_A^-/Q_A)$, of each quinone in the Q_A site. Then the $-\Delta G^\circ_{AB}$ for the $P^+XQ_A^-UQ_B$ to $P^+XQ_AUQ_B^-$ reaction can be calculated, relative to that found in the native UQ_A-containing RCs, given the difference in $E_m(XQ_A^-/XQ_A)$ and $E_m(UQ_A^-/UQ_A)$. The $E_m(Q_B^-/Q_B)$ is assumed to be independent of the quinone in the Q_A site.

(A) Electron transfer from Q_B to P^+ can occur directly at k_{BP} or indirectly through rereduction of Q_A at k_{BAP} (Figure 1). By the latter path $P^+Q_B^-$ and $P^+Q_A^-$ are assumed to remain at equilibrium ($K_{BA} = [P^+Q_AQ_B^-]/[P^+Q_A^-Q_B]$). The observed rate of return to the ground state in $P^+Q_B^-$ RCs (k_{BP}^{obs}) is (*15, 16*)

$$k_{BP}^{obs} = k_{BP} + k_{BAP} = k_{BP} + k_{AP}/(K_{AB} + 1) \quad (1)$$

The direct electron tunneling reaction from Q_B to P^+ occurs at k_{BP}. When $-\Delta G^\circ_{AB}$ is smaller than 100 meV, as in native RCs, the indirect route for charge recombination via Q_A is faster than k_{BP} and $k_{BP}^{obs} \approx k_{BAP}$ (Figure 1). Thus, $-\Delta G^\circ_{AB} = kT \ln(K_{AB})$.

(B) When $-\Delta G^\circ_{AB}$ is greater than 100 meV $k_{BP}^{obs} \approx k_{BP} \gg k_{BAP}$. The direct route is relatively insensitive to $-\Delta G^\circ_{AB}$, so k_{BP}^{obs} no longer provides a monitor of the free energy of the $P^+Q_B^-$ state. This slow, $-\Delta G^\circ_{AB}$-independent charge-recombination reaction is found when the Q_A site in RCs is reconstituted with low potential quinones and with the M265IT mutant even with UQ in the Q_A site. Here, $-\Delta G^\circ_{AB}$ must be found from the energy level of the $P^+Q_A^-$ state relative to P* or P^+H^-. The in situ redox potentials $E_m(Q_A^-/Q_A)$ of different quinones at the Q_A site can be obtained by two different measurements.

(B1) Delayed fluorescence. $P^+Q_A^-$ and P* remain in equilibrium during the lifetime of $P^+Q_A^-$. Earlier studies used single photon counting to monitor the concentration of P* from the amplitude of the fluorescence that has the same lifetime as $P^+Q_A^-$ (*29*). This provided the energy of $P^+XQ_A^-$ relative to P* which was compared with values when UQ_{10} was Q_A. If the free energies of P* and $P^+UQ_B^-$ are independent of the occupant of the Q_A site, the change in the energy level of $P^+XQ_A^-$ provides the change in $-\Delta G^\circ_{AB}$. This method was used for RCs with Me_2NQ and Me_3NQ as Q_A.

(B2) Charge recombination at k_{AHP}. The back-reaction from Q_A^- also has two pathways, k_{AP} where the electron goes back directly to P^+ and k_{AHP} where the electron goes back to P^+ via the higher energy state P^+H^- which returns to the ground state at k_{HP} ($7 \times 10^7\ s^{-1}$) (Figure 1). On the uphill path $P^+Q_A^-$ and P^+H^- remain at equilibrium ($K_{AH} = [P^+H^-Q_A]/[P^+HQ_A^-]$). Thus, the observed back-reaction rate k_{AP}^{obs} is (*29, 31*)

$$k_{AP}^{obs} = k_{AP} + k_{AHP} = k_{AP} + k_{HP}/(K_{AH} + 1) \quad (2)$$

In native UQ_A RCs K_{AH} is so unfavorable that $k_{AP} \gg k_{AHP}$ and the reaction rate is relatively independent of the free energy of Q_A. However, when the energy of the Q_A state is ≈100 meV higher than that of the native UQ, the uphill route dominates k_{AP}^{obs} (*29*, *31*). Here k_{AP}^{obs} can be used to obtain the relative energy of the $P^+HQ_A^-$ and $P^+H^-Q_A$ states. Given that the free-energy levels of P^+H^- and $P^+Q_B^-$ are independent of the occupant of the Q_A site, the change in the energy level of $P^+XQ_A^-$ provides the change in $-\Delta G^\circ_{AB}$. $P^+Me_4NQ_A^-$ was determined to be 120 meV less stable than $P^+UQ_{10}^-$ given $k_{AP}^{obs} = 25.0\ s^{-1}$.

Determining Which Quinone Occupies the Q_A and Q_B Sites. The goal is to prepare all RCs with non-native quinones (generically referred to as XQ) in the Q_A site (XQ_A) and ubiquinone in the Q_B site (UQ_B) (XQ_AUQ_B RCs). However, the different quinones and UQ compete for the Q_A site and UQ binds more tightly to the Q_A site than to the Q_B site. Thus, adding too much UQ displaces XQ_A yielding UQ_AUQ_B RCs. Adding too little UQ leaves a large fraction of RCs without Q_B (XQ_A RCs). The optimal concentration of UQ to be added was calculated at an XQ concentration near the solubility limit of the exogenous quinone from the known dissociation constants of XQ and UQ for the Q_A and Q_B sites (*32*) (see Appendix).

The assay solution contained 4−5 μM RCs with 0.02% Triton X-100, 2.5 mM KCl, and 10 mM Tris buffer at pH 7.8−8.0. Following complete reconstitution of the Q_A site with the replacement quinone, the sample solution was split to provide two matched samples for comparison of Q_A- and Q_AQ_B-containing RCs. Q_B was reconstituted with UQ (UQ_B). When Q_A was a quinone which would bind tightly to the Q_A site, Q_B was reconstituted with ≈12−15 UQ_{10} per RC. If UQ_{10} would displace the loosely bound NQs at Q_A, 2−6 UQ_1 per RC was used to reconstitute Q_B. The final UQ_B occupancy was about 95% when UQ_{10} was used and more than 80% when UQ_1 was Q_B.

Addition of XQ and UQ generally yields a mixture of RCs with XQ_A, UQ_A, XQ_AUQ_B, and UQ_AUQ_B. The kinetics of charge recombination was used to determine the relative occupancy of each quinone in each binding site. After an activating flash, four types of RCs are formed when both UQ and XQ are added: $P^+XQ_AUQ_B^-$, $P^+UQ_AUQ_B^-$, and when the Q_B site is empty, $P^+XQ_A^-$ and $P^+UQ_A^-$. The values of k_{AP}^{obs}, the rate of charge recombination from Q_A^- to P^+, and k_{BP}^{obs}, the rate from Q_B^- to P^+, are different for RCs with each quinone complement (Table 1). The rates in the last three types of RCs were measured in samples with only UQ or XQ added. With the different XQ_As, k_{AP}^{obs} ranges from 6 to 400 s^{-1} and k_{BP}^{obs} from 2 to 0.1 s^{-1}. Analyses of charge-recombination kinetics in RCs with mixtures of quinones fix these pre-established rate constants, while k_{BP}^{obs} in the $P^+XQ_AUQ_B^-$ is a free parameter (Figure 2). The amplitude of the kinetic component associated with XQ_AUQ_B RCs ranged from 45% to 80% in the R-26 RCs with different XQs added.

For the mutant M265IT RCs it is impossible to determine the fraction of XQ_AUQ_B and UQ_AUQ_B RCs from the kinetics of charge recombination. When both Q_A and Q_B sites are occupied by UQ_{10}, the estimated free energy for $-\Delta G^\circ_{AB}$ is greater than 120 meV so that charge recombination occurs by direct electron transfer to P^+ at k_{BP} rather than indirectly via Q_A (k_{BAP}^{obs}). In this case k_{BP}^{obs} is indistinguishable in $P^+XQ_AUQ_B^-$ or $P^+UQ_AUQ_B^-$ RCs.

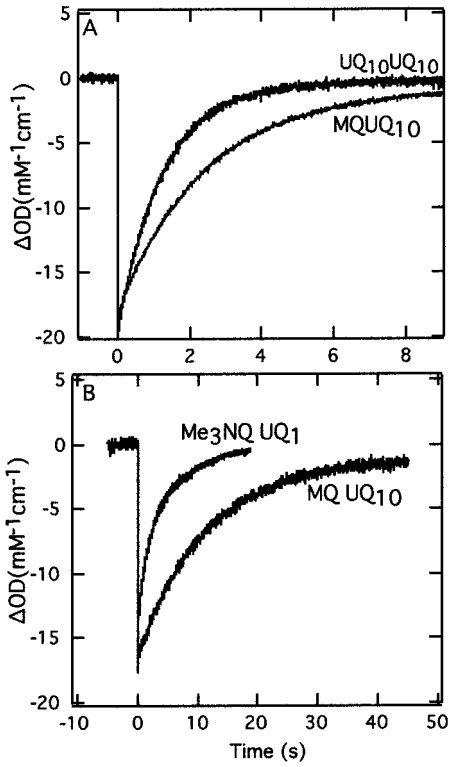

FIGURE 2: Determination of the distribution of quinones in each binding site from the kinetics of charge recombination. Absorbance changes at 430 nM, a maximum for the difference between P^+ and P absorbance in the near UV, monitor the oxidation state of P. (A) Upper trace: UQ_{10} only added yields UQ_AUQ_B RCs with >95% UQ_{10} at both sites. k_{BP}^{obs} can be fit with a single rate constant of 0.85 s^{-1}, showing only the reaction characteristic of $P^+UQ_AUQ_B^-$ RCs. Lower trace: MQ (vitamin K_1) and UQ_{10} added. k_{BP}^{obs} is 80% at 0.36 s^{-1} (MQ_AUQ_B RCs) and 20% at 0.85 s^{-1} (UQ_AUQ_B RCs). The rate constant of 0.85 s^{-1} for the UQ_AUQ_B RCs was fixed, but k_{BP}^{obs} for the $MQ_AUQ_B^-$ RCs and the distribution of RCs with each quinone complement are derived from the kinetic analysis. (B) Top: Me_3NQ and UQ_1 added to R-26 RCs. Charge recombination fitted with fixed rates for k_{AP}^{obs} for UQ_1 at Q_A with no Q_B, 6.9 s^{-1} (10%); Me_3NQ at Q_A with no Q_B, 16 s^{-1} (15%); k_{BP}^{obs} with UQ_1 at Q_A and Q_B, 1.7 s^{-1} (14%). The value for k_{BP}^{obs} in $Me_3NQ_AUQ_B$ RCs is found to be 0.19 s^{-1} (61%). Bottom: MQ and UQ_{10} added to M265IT RCs. The charge recombination rate, k_{BP}^{obs}, is 0.1 s^{-1} (95%). All samples contain 4 μM RCs, 0.02% Triton, 10 mM Tris, 2.5 mM KCl at 22 °C, and have a pH of 8.0.

Although the XQ concentration is many times that of the RCs, the presence of XQ_B is considered to be unimportant. First, when only naphthoquinones are added there is never electron transfer from a naphthoquinone in the Q_A site to a naphthoquinone in the Q_B site (*33*). Second, the electron transfer from UQ_A^- to XQ_B would always be energetically uphill with the quinones used here and so would not contribute to the results. Last, XQ does not appear to compete significantly with UQ for the Q_B site at the concentration of XQ used here.

RESULTS

Determining $k_{AB}^{(1)}$ in XQ_AUQ_B RCs. Time-resolved absorption changes due to the electron transfer from XQ_A^- to UQ_B in the R-26 and M265IT RCs were measured at 400,

406, and 470 nm after an actinic laser flash. The difference between the absorbance of a naphthoquinone as Q_A and ubiquinone as Q_B has its maximum at 400 nm (*10*). This is also an isobestic point in the absorbance difference between P and P^+, so the large absorbance changes from P oxidation do not add to the signal. However, there is a significant contribution at this wavelength from the UQ_A^- to UQ_B electron-transfer reaction in RCs where UQ has replaced XQ in the Q_A site. Isobestic points in the UQ_A^- vs UQ_B^- spectra are found at 406 and 470 nm. Here, electron transfer from XQ_A^- to UQ_B can be seen, but the reaction in contaminating UQ_AUQ_B RCs cannot.

The first state to be seen after the flash is $P^+XQ_A^-UQ_B$ (Figure 3). This either evolves into $P^+XQ_AUQ_B^-$ (at $k_{AB}^{(1)}$) or returns to the ground state (at k_{AP}^{obs}). The rate k_{AP}^{obs} is determined in matched samples without UQ added (Table 1). There is a third, slow kinetic component in Q_B-containing RCs that was described previously (*10*, *34*). However, this is seen only near 400 and not at 406 or 470 nm. This slow component appears to monitor a process occurring after the electron transfer from Q_A^- to Q_B (see ref *10* for a more complete description).

The two components of the rate of electron transfer from Q_A^- to UQ_B ($k_{AB}^{(1)}$) and their uncertainties are listed in Table 1 for RCs with different XQ_As. Figure 3 shows the fast kinetic component in RCs containing Me_3NQ as Q_A and UQ_1 as Q_B. The lifetime of 0.39 μs is assigned to the XQ_A^- to UQ_B electron-transfer reaction (Figure 3a,b). With Me_3NQ alone at the Q_A site and no UQ_B, there is no change in the optical absorption for 1 ms at 400 and 470 nm (data not shown).

Effects of the Free Energy ($-\Delta G^\circ_{AB}$) *on the Electron-Transfer Kinetics.* The rate of the fastest phase is compared for RCs with $-\Delta G^\circ_{AB}$ from 60 to 250 meV. The variation in the reaction driving force is obtained by use of naphthoquinones with different in situ electrochemical midpoints as Q_A. This rate is dependent on $-\Delta G^\circ_{AB}$, changing by a factor of $\approx$10 for each 100 meV (Figure 4). As found previously (*7*) the $\approx$100 μs phase is independent of $-\Delta G^\circ_{AB}$, with an average lifetime τ_2 of 110 $\pm$ 35 μs ((9.1 $\pm$ 2.6) $\times$ 10^3 s^{-1}).

Effects of the Free Energy ($-\Delta G^\circ_{AB}$) *on the Amplitude of the Fast Phase.* In the RCs where the various NQs are used in the Q_A site, the fraction of the reaction occurring in the fast phase varies from 22 to 100%, increasing with $-\Delta G^\circ_{AB}$. Thus, as the driving force increases and the rate of electron transfer increases, the fraction of the reaction occurring at τ_1 increases (Figure 5). However, in R-26 or M265IT RCs when UQ_{10} was both Q_A and Q_B, τ_1 accounts for less than 10% of the reaction.

Influence of the Number of Isoprene Units on the Quinone at the Q_A Site. Menaquinone with 2, 4, and 10 isoprene tails was substituted in the Q_A site with UQ_{10} as Q_B. In each case k_{BP}^{obs} is essentially the same. Because charge recombination is via the free-energy-dependent indirect route, k_{BAP} (eq 1), this ensures that $-\Delta G^\circ_{AB}$ is independent of the length of the tail on Q_A.

Changing the tail length of the menaquinone at Q_A results in small changes in the lifetime and amplitude of the fast phase of the electron transfer from Q_A^- to Q_B. τ_1 decreases 2-fold as the tail lengthens from 2 to 10 isoprene units (Figure 6). At the same time the fraction of the reaction that occurs

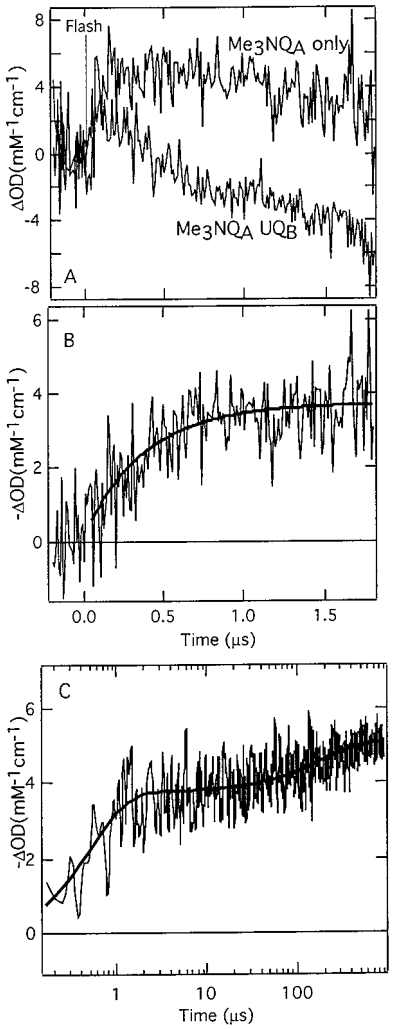

FIGURE 3: Optical absorbance changes associated with electron transfer from Me_3NQ as Q_A to UQ_1 as Q_B in R-26 RCs. (A) A 10-μs xenon flash provides the measuring light. The signal was monitored at 400 nm. Differences from the ground-state absorbance: top curve, $P^+Me_3NQ_A^-$ RCs, no UQ_1 added; bottom curve, change in absorbance as RCs go from $P^+Me_3NQ_A^-$ to $P^+Me_3NQ_AUQ_B^-$ states. (B) $P^+Me_3NQ_A^-$ trace subtracted from $P^+Me_3NQ_AUQ_B^-$ showing only the electron transfer from Me_3NQ_A to UQ_B. The data are fit to a single exponential with $\tau_1 = 0.39$ μs ($k_1 = 2.6 \times 10^6$ s^{-1}). (C) A continuous measuring lamp monitors the absorbance at 470 nm, which is an isobestic point in the difference spectra of UQ_A^- and UQ_B^-. The $P^+(Me_3NQ)_A^-(UQ_1)_B \rightarrow P^+(Me_3NQ)_A(UQ_1)_B^-$ kinetic trace is subtracted from a matched control sample without UQ_B added ($P^+(Me_3NQ)_A^-$). This can be fit with two exponentials (solid line) with $\tau_1 = 0.52$ μs (k_1 = (1.94 $\pm$ 0.22) $\times$ 10^6 s^{-1}) (75%), $\tau_2 = 200$ μs (25%). Sixty transients were averaged.

at τ_1 decreases from 45% to 22%, while the fraction of the reaction occurring at τ_2 increases (Figure 6).

Influence of Number of Isoprene Units on the Ubiquinone at the Q_B Site on the Rate of ElectronTransfer from XQ_A^- to UQ_B. A series of UQ homologues was substituted at the Q_B site in RCs with vitamin K_1 (MQ) as Q_A. Given the variation in k_{BP}^{obs}, $-\Delta G^\circ_{AB}$ is found to increase from 72 meV with UQ_1 to 93 meV with UQ_{10} as Q_B (Table 1). In this series the lifetime of the fast phase of electron transfer from Q_A^- to Q_B (τ_1) decreases as the tail on UQ_B is lengthened (Figure 7). The rate of the slower reaction (τ_2) is independent of the tail length of UQ_B.

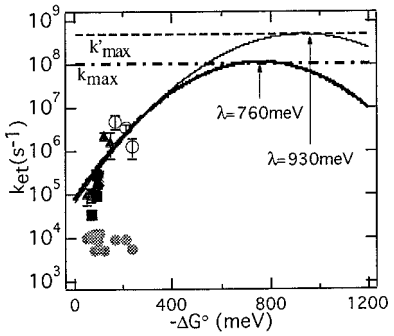

FIGURE 4: $-\Delta G^{\circ}_{AB}$ Dependence of the rate constant of the fast and ≈100-μs phase at 22 ± 1 °C of the electron transfer from Q_A^- to Q_B. The average values of the rate constants have been plotted. The Marcus parabola were drawn using eq 3 with $\lambda = 760 \pm 30$ meV and $V(r) = 1.1 \times 10^{-8}$ eV ($k_{max} = 1.1 \times 10^8$ s^{-1} from Moser and Dutton); or $\lambda = 930 \pm 30$ and $V(r) = 1.7 \times 10^{-7}$ eV (k'_{max} of 5×10^8 s^{-1} from Calvo et al. (*44*)). The gray circles are the slower rate for RCs with each quinone (the ≈100-μs phase, k_2). The black symbols are the fast component of the reaction in the RCs with a wild-type Q_A site: (■) MQ at the Q_A site with UQs with different length tails as Q_B; (▼) NQs with different tail lengths at the Q_A site; and (▲) methyl-substituted NQs as Q_A. The open circles are the fast component of the reaction in the M265IT RCs.

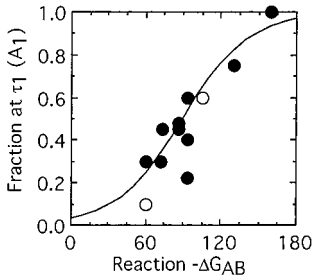

FIGURE 5: Fraction of the electron-transfer reaction that occurs in the fast phase, A_1, as a function of $-\Delta G^{\circ}_{AB}$. Data determined at 406 or 470 nm. (A) The theoretical line assumes the fast phase represents a burst phase where Q_A^- comes to equilibrium with an unrelaxed form of Q_B^- at an observed rate ($\tau_1 + \tau_{-1}$). This state is 90 meV higher in energy than the equilibrated form of Q_B^-. The initial fraction of the protein in the Q_B^{-}* state is $[Q_B^{*-}]/([Q_A^-] + [Q^{*-}]) = K_{eq}/(K_{eq} + 1)$ where $K_{eq} = ([Q_A^-]/[Q_B^{-}*])$. Q_B^{-}* relaxes at τ_2 (≈100 μs). (●) XQ_AUQ_B RCs; (○) UQ_AUQ_B RCs, 60 meV in isolated protein and at 105 meV in chromatophores (*8*).

UQ_0 was also tried as UQ_B. Here, the electron transfer from Q_A^- to Q_B is slow and shows a negligible amount of electron transfer at τ_1. This is because the affinity of UQ_0 for the Q_B site is so small that the site is not fully occupied. Thus, binding UQ_0 to the Q_B site is the rate-limiting step. As expected, the rate of electron transfer is now dependent on the UQ_0 concentration (*30*).

pH Dependence of the Electron Transfer from Q_A to Q_B in MQ_AUQ_B RCs. The fast reaction was measured as a function of pH in MQ_AUQ_B RCs. The lifetime τ_1 is pH independent from pH 6 to 11 (Figure 8). Thus, proton binding from solution is not the rate-limiting step even at high pH. In contrast, the slower components are pH dependent. τ_2 is essentially constant at ≈100 μs at low pH. This phase of the reaction slows as the pH is increased beyond pH 8. The lifetime of the very slow kinetic component, τ_3, seen at 400 nm, also increases at high pH where it is on the order of milliseconds. The pH dependences of τ_2, τ_3, and their relative amplitudes are consistent with previous studies (*16*, *35*).

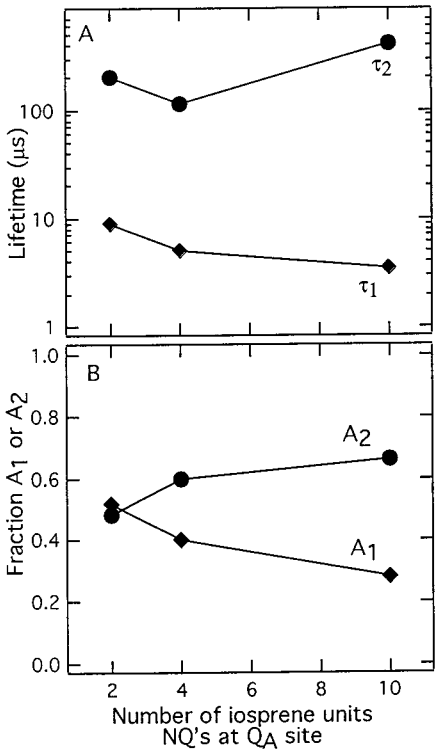

FIGURE 6: Influence of the number of isoprene units on the naphthoquinone in the Q_A site on the rate and amplitude of each phase of electron transfer from Q_A^- to Q_B. UQ_{10} is Q_B in all cases. Measured at 400 nm and pH 8, R-26 RCs. (A) Lifetimes τ_1 and τ_2, (B) Fraction of the reaction occurring at τ_1 (A_1) and τ_2 (A_2).

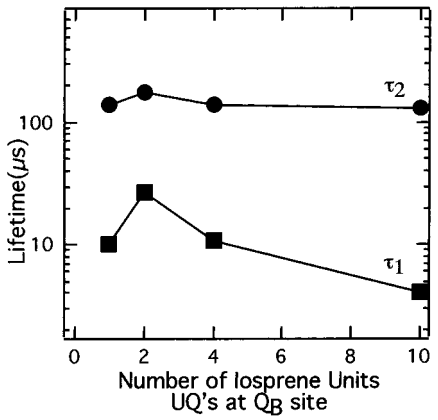

FIGURE 7: Influence of the number of isoprene units on the UQ at the Q_B site on the rate of each of phase of electron transfer from Q_A^- to Q_B. MQ (vitamin K_1) was Q_A in all cases. Measured at 406 nm and pH 8, R-26 RCs. Lifetimes τ_1 (◆) and τ_2 (●).

DISCUSSION

The electron transfer from Q_A^- to Q_B can occur in several distinct kinetic phases. Thus, in addition to the well-studied process that occurs at ≈100 μs (τ_2 here), a faster reaction can be seen (τ_1). With naphthoquinones in the Q_A site, the fast phase is found in isolated *Rb. sphaeroides* RCs. It is seen in protein with native quinone binding sites such as the R-26 strain used here, and in the M265IT mutant where an Ile in the Q_A site was changed to Thr (*25*). A previous study demonstrated that in MQ_AUQ_B RCs the spectral changes associated with τ_1 are consistent with the difference spectra between the semiquinones MQ^- and UQ^- in solution

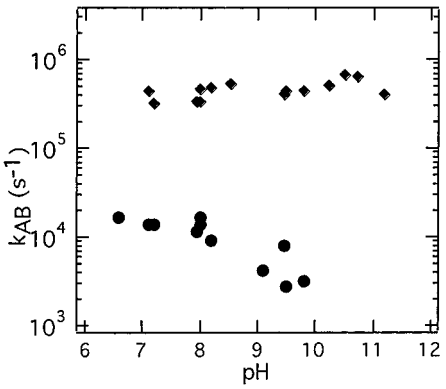

FIGURE 8: pH dependence of the rate of each phase of electron transfer from Q_A^- to Q_B. R-26 RCs with MQ as Q_A and UQ_{10} as Q_B, measured at 400 nm. Lifetimes τ_1 (●) and τ_2 (◆).

(*10*). Thus, this phase monitors electron transfer from Q_A^- to Q_B. Fast phases are also seen in chromatophores of *Rb. sphaeroides* with the native UQ as Q_A (*8*) and in *Rb. viridis* chromatophores where menaquinone is the native Q_A (*36, 37*).

The fast phase of electron transfer behaves differently from the ≈100 μs process. The fast reaction is free-energy dependent (Figure 4), whereas the ≈100 μs process is not (*7*). Thus, as will be described below, the fast reaction rate can be used to characterize the electron-transfer reaction itself. In contrast, the ≈100 μs component is gated by some other process which may be proton, protein, or cofactor motion. The fast rate is pH independent up to pH 11. The ≈100 μs component is pH independent only up to pH 8 and then slows with increasing pH (*16, 34*). In *Rhodopseudomonas viridis* chromatophores where menaquinone is Q_A and ubiquinone is Q_B, the primary phase of the electron transfer from Q_A to Q_B has a lifetime of 20 μs. This reaction also remains pH independent at alkaline pH (*36, 37*).

Analysis of the Dependence of the Electron Transfer from Q_A^- to Q_B on $-\Delta G^\circ_{AB}$. The electron-transfer reactions in RCs have provided much of the available information about the free-energy and distance dependence of electron transfer in proteins (*38, 39*). RCs are a good system for study for several reasons. First, there are many reactions that can be measured, each with a different distance, rate, and driving force. In addition, several methods allow the driving force for each to be changed. These include cofactor replacement and protein mutation, both of which are used here, as well as application of electric fields across the protein (*40, 41*). The free-energy dependence of the electron-transfer reactions can be analyzed by theories derived from Marcus electron-transfer theory (*42, 43*). It has not been possible to analyze the underlying electron transfer from Q_A^- to Q_B previously because the well-studied ≈100 μs component is independent of $-\Delta G^\circ_{AB}$. However, the fast phase appears to have an appropriate dependence on $-\Delta G^\circ_{AB}$. In Marcus electron-transfer theory the electron-transfer rate is

$$k_{ET} = \frac{4\pi^2|V(r)|^2}{h\sqrt{4\pi\lambda k_B T}} \exp\left[-\frac{(\Delta G^\circ_{ET} + \lambda)^2}{4\lambda k_B T}\right] = k_{max} \exp\left[-\frac{(\Delta G^\circ_{AB} + \lambda)^2}{4\lambda k_B T}\right] \quad (3)$$

where $-\Delta G^\circ_{ET}$ is the free energy for electron transfer (defined as the energy of the final minus the initial state, $-\Delta G^\circ_{AB}$ in this work), and $V(r)$ is the electronic coupling between the initial and final states. Equation 3 assumes that the electron-transfer process is in the high-temperature limit, where the thermal energy (k_BT) is much larger than the energy of the vibrations coupled to the process ($h\omega$); k_{max} is the maximum rate of electron transfer when the atoms of the system are correctly arranged for reaction (when $-\Delta G^\circ_{ET} = \lambda$).

As with all analysis of the free-energy dependence of the rate it is necessary to assume that the primary change when the various NQs are substituted for UQ in the R-26 or M265IT RCs is in $-\Delta G^\circ_{AB}$. Thus, changes in λ and $V(r)$ are assumed to be minimal. The use of several RCs which achieve similar $-\Delta G^\circ_{AB}$ values by different combinations of modifications provide some control for changes in parameters other than $-\Delta G^\circ_{AB}$.

In this study, $-\Delta G^\circ_{AB}$ is changed from 50 to 240 meV and the rate changes by 25-fold from 9×10^4 to 2.3×10^6 s^{-1}. Unfortunately, this $-\Delta G^\circ_{AB}$ range does not extend to sufficiently negative values to allow determination of both $V(r)$ and the reorganization energy. Here, $V(r)$ was fixed given estimates of the maximum rate of electron transfer (k_{max}) from Q_A^- to Q_B derived from other sources (Figure 4). The value for λ was then obtained from the free-energy dependence of k_1 determined here. Calvino et al. (*44*) determined k_{max} to be 5×10^8 s^{-1} from the magnetic coupling between the spins on Q_A^- and Q_B^- in RCs where both quinones are reduced (in the $Q_A^-Q_B^-$ state). This yields a $V(r)$ of 1.7×10^{-8} eV and a λ of 930 ± 30 meV. Moser and Dutton (*60*) estimated k_{max} to be 1.1×10^8 s^{-1} given the distance from Q_A^- to Q_B and the packing of the protein between these two sites. This yields a $V(r)$ of 7.6×10^{-8} eV and a λ of 760 ± 30 meV. The estimated errors are based upon standard deviations of the least-squares fit of the data to eq 3. Given $V(r)$ the data can be fit to the Marcus formula with only small error. But the estimate of λ presented here relies on the value of $V(r)$. The two available estimates, derived by different methods, provide values of $V(r)$ that differ by less than a factor of 5 and yield values of λ that differ by 170 meV.

The reorganization energy for the fast phase of electron transfer from Q_A^- to Q_B is ≈850 ± 100 meV given $V(r)$ of $(1.7-7.6) \times 10^{-8}$ eV. Previously determined values for reactions involving Q_A or Q_B in RCs provided values of λ for the electron transfer from Q_A^- to P^+ ranging from ≈600 meV in frozen RCs (*45*) to 900 meV (*46*−*48*) at room temperature. At room temperature, λ for the analogous reaction from Q_B^- to P^+ is 1300 meV (*49*). The electron transfer from Q_B^- to P^+ has significantly larger reorganization energy than that from Q_A^- to P^+. Thus, RCs in the relaxed $P^+Q_B^-$ state appear to differ more from the ground state than does the protein in the $P^+Q_A^-$ state. Significant change on forming $P^+Q_B^-$ is consistent with the slow conformational gate seen in the ≈100 μs phase of the reaction. In contrast, the relatively small λ for the fast phase of electron transfer from Q_A^- to Q_B suggests that this phase of the reaction occurs with more modest rearrangement.

A Kinetic Model That Yields the Observed Amplitude of the Fast (k_1) and Slow (k_2) Phases of Electron Transfer from Q_A^- to Q_B. The amplitude of the fast phase of electron

transfer from Q_A^- to Q_B varies with different XQ_A's. As the $-\Delta G^\circ_{AB}$ and the fast rate (k_1) increase, the amplitude of the reaction at k_1 increases (Figure 5). This trend is consistent with the substantial amount of fast phase previously found in chromotophores (*8*) and with less seen in isolated RCs. The $-\Delta G^\circ_{AB}$ in chromatophores is ≈105 meV (*50, 51*), wherease it is only 60 meV in native, isolated RCs. The amplitude of fast phase in chromatophores does lie on the line shown in Figure 5. However, there is less fast phase in isolated RCs than expected if the reaction $-\Delta G^\circ_{AB}$ solely determined the partitioning between fast and ≈100 μs phases. The fast phase accounts for less than 15% of the UQ_A to UQ_B reaction, but with Me_2NQ, at the same $-\Delta G^\circ_{AB}$, 30% of the reaction occurs in the fast phase.

In the RCs with UQ_A and UQ_B there are several reasons why the fraction of fast phase could be underestimated. There is no direct marker for the electron transfer from UQ_A to UQ_B, and all of the spectral changes are much smaller in these RCs. It is difficult to get a control sample fully reconstituted with UQ_A with no UQ_B to establish the initial absorbance changes in the Q_A^- state for a particular sample. Also, in the RCs with naphthoquinones with different length tails, the longer the tail, the smaller the fraction of the reaction that occurs at the fast rate. Thus, the UQ_{10} used in the Q_A site here may diminish the amplitude of the fast phase of the reaction.

However, the lack of a fast phase with UQ in the M265IT RCs where the $-\Delta G^\circ_{AB}$ is 160 meV suggests that UQ_AUQ_B RCs may be different from RCs reconstituted with naphthoquinones in the Q_A site. UQ is special in other ways. This is the only quinone that will function as both Q_A and Q_B. Many quinones can reconstitute Q_A (*45, 52*). However, nonnative Q_B's can only be reconstituted in RCs with a low potential Q_A suggesting that $-\Delta G^\circ_{AB}$ is unfavorable for RCs with quinones other than UQ at both sites (*33*). It may be that the unknown, special properties that allow the $-\Delta G^\circ_{AB}$ to be tuned correctly for electron transfer to occur from UQ_A^- to UQ_B also in some way keep the conformational gate closed so that no fast phase in allowed (see ref *10* for additional discussion).

Correlation of the amplitude of the fast reaction with $-\Delta G^\circ_{AB}$ suggests several possible kinetic models consistent with the heterogeneous kinetics. There could be a high-energy Q_B^- state (Q_B^-*) formed without the conformational changes seen in the ≈100 μs reactions. Thus, the fast rate occurs in RCs little changed from that found in the Q_A^- state. If Q_A^- and Q_B^-* rapidly come to equilibrium, the fraction of the fast, burst phase would be determined by the equilibrium constant Q_B^-*/Q_A^-, increasing as the Q_A^- energy increased. The 100 μs phase of the reaction is gated by a conformation change at ≈100 μs (k_2) (*7*) which would then form stable product from either Q_A^- or Q_B^-*. If Q_A^- is much lower in energy than Q_B^-* the burst is too small to be seen, and conformation change provides the only route for electron transfer to Q_B. The data will fit this model with an energy difference of ≈90 meV between Q_B^-* and the final relaxed Q_B^-. Thus, when the Q_A^- is 90 meV above the equilibrated $Q_AQ_B^-$ state, 50% of the reaction occurs in the burst phase. In this model, $-\Delta G^\circ_{AB}$ for the fast phase is 90 meV smaller than that measured at equilibrium. One outcome is that the free energies in the Marcus curve would be shifted, thereby reducing the estimated value of λ. Candidates for the conformational changes gating the reaction could be the motion of the quinone from a distal to proximal binding site (*53*) or changes in ionization and hydrogen bond patterns of residues near Q_B (*54, 55*).

Another kinetic model, with Q_A^- formed in a state that can rapidly transfer an electron to Q_B, is also consistent with the data. Within ≈5 μs this state then relaxes to a form of Q_A^- requiring conformational gating for reduction of Q_B. The partitioning between fast and ≈100 μs phases here represents the competition between electron transfer and relaxation in Q_A^-*. The driving force for electron transfer would be larger than that obtained from equilibrium measurements. This model has initially excited RCs formed in a state that allows electron transfer with relaxation trapping $P^+Q_A^-Q_B$. Fast proton binding near Q_A (*56, 57*) or even near Q_B (*58, 59*) might account for the inactivation. In contrast, the kinetic model which postulates Q_B^-* assumes that the ground and $P^+Q_A^-Q_B$ RCs are not competent to form the normal product Q_B without some changes. Thus, while patterns are emerging from the study of the fast phase of this reaction, the underlying mechanism that partitions the reaction between fast and ≈100 μs phases cannot yet be assigned.

ACKNOWLEDGMENT

We thank Colin Wraight, Mel Okamura, Mike Graige, Armen Mulkidjanian, and Chris Moser for helpful discussions.

APPENDIX: MODEL FOR COMPETITIVE BINDING OF XQ TO Q_A AND UBIQUINONE TO Q_A AND Q_B SITES

The goal is to prepare samples with the maximum fraction of RCs with XQ_A and UQ_B. However, XQ and UQ compete for the Q_A site. In addition, UQ binds more tightly to the Q_A site than to the Q_B site and binds more tightly than some XQs to the Q_A site. Thus, adding too much UQ will yield RCs with UQ_A, whereas adding too little UQ will leave RCs with an empty Q_B site.

The optimal concentration of UQ to produce the maximum fraction of RCs with XQ_AUQ_B can be calculated because the equilibrium dissociation constants (K_D) are known for the different XQs at the Q_A site, UQ at the Q_A site, and UQ at the Q_B site. The equilibrium RC quinone complement is obtained by assuming the following: (1) Binding of a UQ to Q_B does not depend on whether a UQ or XQ is at Q_A. (2) Because of the difference in affinities, UQ never binds to the Q_B site if the Q_A site is unoccupied. (3) Naphthoquinones (XQs) do not bind to the Q_B site.

For the calculations, X represents the concentration of XQ, R the RC concentration, R_x RCs with XQ bound at Q_A, U UQ, R_u RCs with UQ bound at Q_A, R_b RCs with XQ or UQ bound at Q_A and UQ bound at Q_B, R_t the total RC concentration, R_f RCs with no quinone bound, X_t the total XQ concentration, X_f the concentration of free XQ in the solution, U_t the total UQ quinone concentration, and U_f the free UQ concentration. $(R_x + R_u)_f$ are RCs with their Q_A sites occupied, but with empty Q_B sites. K_x, K_a, and K_u are the dissociation constants for XQ at the Q_A site, UQ at the Q_A site, and UQ at the Q_B site, respectively. The percentage of XQ_AUQ_B RCs is $(R_xR_u/(R_xR_u)R_t)$.

At equilibrium,

(XQ binds to Q_A) $$X + R \leftrightarrow R_x \quad \text{(A1)}$$

(UQ binds to Q_A) $$U + R \leftrightarrow R_u \quad \text{(A2)}$$

(UQ binds to Q_B) $$U + (R_x + R_u) \leftrightarrow R_b \quad \text{(A3)}$$

$$K_x = \frac{X_f R_f}{R_x} \quad \text{(A4)}$$

$$K_u = \frac{U_f R_f}{R_u} \quad \text{(A5)}$$

$$K_b = \frac{U_f (R_x + R_u)_f}{R_b} \quad \text{(A6)}$$

$$R_t = R_f + R_x + R_u \quad \text{(A7)}$$

$$X_t = X_f + R_x \quad \text{(A8)}$$

$$U_t = U_f + R_u + R_b \quad \text{(A9)}$$

$$(R_x + R_u)_f = R_x + R_u - R_b \quad \text{(A10)}$$

Rearranging,

$$R_f = R_t - R_x - R_u \quad \text{(A11)}$$

$$X_f = X_t - R_x \quad \text{(A12)}$$

$$U_f = U_t - R_u - R_b \quad \text{(A13)}$$

$$R_f X_f = K_x R_x \quad \text{(A14)}$$

$$R_f U_f = K_u R_u \quad \text{(A15)}$$

$$U_f (R_x + R_u - R_b) = K_b R_b \quad \text{(A16)}$$

These can be simplified further:

$$U_t - R_u - R_b = \frac{K_b R_b}{(R_x + R_u - R_b)} \quad \text{(A17)}$$

$$R_t - R_x - R_u = \frac{K_u R_u}{K_b R_b}(R_x + R_u - R_b) \quad \text{(A18)}$$

$$X_t - R_x = \frac{K_x K_b R_x R_b}{K_u R_u (R_x + R_u - R_b)} \quad \text{(A19)}$$

The concentration of R_x can be determined from:

$$0 = -(b^2c^3s^2) + (abc^2rs - 2b^2c^2rs + 3b^2c^2s^2 + 2bc^3s^2 + 2bc^2rs^2 - bc^2rst)R_x + (-2abcrs + 4b^2crs - ac^2rs + 3bc^2rs - acr^2s + 4bcr^2s - 3b^2cs^2 - 6bc^2s^2 - c^3s^2 - 4bcrs^2 - 2c^2rs^2 - cr^2s^2 + acr^2t - bcr^2t + {}^2bcrst + c^2rst + cr^2st)R_x^2 + (abrs - 2b^2rs + 2acrs - 6bcrs - c^2rs + ar^2s - 4br^2s - 3cr^2s - 2r^3s + b^2s^2 + 6bcs^2 + 3c^2s^2 + 2brs^2 + 4crs^2 + r^2s^2 + ar^2t + br^2t + cr^2t + r^3t - brst - 2crst - r^2st)R_x^3 + (-(ars) + 3brs + 2crs + 3r^2s - 2bs^2 - 3cs^2 - 2rs^2 - r^2t + rst)R_x^4 + (-(rs) + s^2)R_x^5 \quad \text{(A20)}$$

where $a = U_t$, $b = R_t$, $c = X_t$, $r = K_x$, $s = K_u$, $t = K_b$. The numerical solution of eq 20 can be obtained with Mathematica software (Wolfram). Given R_x, the concentration of RCs with XQ_A, R_u, the concentration with UQ_A, and R_b, the concentration with UQ_B, the following can be obtained (Figure A1):

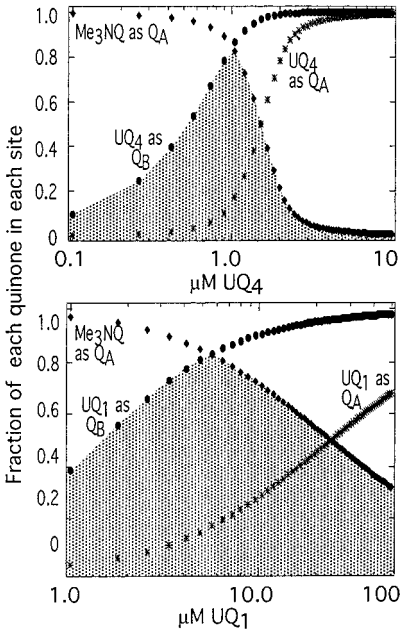

FIGURE A1: Concentrations of RCs with Me_4NQ as XQ, and UQ_1 and UQ_4 as UQ. R_x, R_u, and R_b were determined as a function of the concentration of UQ_1 or UQ_{10} at fixed XQ concentration. With $R_t = 1$ μM, XQ = 20 μM (Me_4NQ), a concentration near the solubility limit for this quinone. At Q_A: $K_x = 0.06$ μM (Me_4NQ), $K_{u4} = 0.00024$ μM (UQ_4), $K_u = 0.085$ μM (UQ_1). At Q_B: $K_u = 0.002$ μM (UQ_4), $K_u = 1$ μM (UQ_1). Top: With UQ_4 and 10 μM Me_4NQ, the maximum concentration of XQ_AUQ_B RCs is 80% of the total RCs. This is found in a narrow range of concentration peaked at 1 μM UQ_4. Bottom: With UQ_1, which binds more weakly to the RCs, a similar maximum XQ_AUQ_B fraction can be achieved at $\approx$6 μM UQ. However, the range of concentrations where a substantial fraction of RCs has the desired quinone complement is much larger.

$$R_u = \frac{R_t R_x - (R_t + X_t + K_x)R_x + R_x^2}{X_t - R_x} \quad \text{(A21)}$$

$$R_b = \frac{K_u R_x (R_x + R_u)}{(R_t - R_x - R_u)K_b + K_u R_u} \quad \text{(A22)}$$

REFERENCES

1. Feher, G., Allen, J. P., Okamura, M. Y., and Rees, D. C. (1989) *Nature 339*, 111−116.
2. Gunner, M. R. (1991) *Curr. Top. in Bioenerg. 16*, 319−367.
3. Blankenship, R. E., Madigan, M. T., and Bauer, C. E. (1995) *Anoxygenic Photosynthetic Bacteria*, Vol. 2, Kluwer Academic Publishers, Boston, MA.
4. Kirmaier, C., and Holten, D. (1993) in *The Photosynthetic Reaction Center* (Deisenhofer, J., and Norris, J. R., Eds.) pp 49−70, Academic Press, San Diego, CA.
5. Kleinfeld, D., Okamura, M. Y., and Feher, G. (1985) *Biochim. Biophys. Acta 809*, 291−310.
6. Okamura, M. Y., and Feher, G. (1995) in *Anoxygenic Photosynthetic Bacteria* (Blankenship, R., Madigan, M., and Bauer, C., Eds.) pp 577−593, Kluwer Academic Publishers, Dordrecht, The Netherlands.
7. Graige, M. S., Feher, G., and Okamura, M. Y. (1998) *Proc. Natl. Acad. Sci. U.S.A. 95*, 11679−11684.
8. Tiede, D. M., Vazquez, J., Cordova, J., and Marone, A. P. (1996) *Biochemistry 35*, 10763−10775.

9. Tiede, D. M., Utschig, L., Hanson, D. K., and Gallo, D. M. (1998) *Photosynth. Res. 55*, 267−273.
10. Li, J., Gilroy, D., Tiede, D. M., and Gunner, M. R. (1998) *Biochemistry 37*, 2818−2829.
11. Lavergne, J., Matthews, C., and Ginet, N. (1999) *Biochemistry 38*, 4542−4552.
12. Vermeglio, A., and Clayton, R. K. (1977) *Biochim. Biophys. Acta 461*, 159−165.
13. Lubitz, W., Abresch, E. C., Debus, R. J., Isaacson, R. A., Okamura, M. Y., and Feher, G. (1985) *Biochim. Biophys. Acta 808*, 464−469.
14. Wraight, C. A. (1979) *Biochim. Biophys. Acta 548*, 309−327.
15. Mancino, L. J., Dean, D. P., and Blankenship, R. E. (1984) *Biochim. Biophys. Acta 764*, 46−54.
16. Kleinfeld, D., Okamura, M. Y., and Feher, G. (1984) *Biochim. Biophys. Acta 766*, 126−140.
17. Maroti, P., and Wraight, C. A. (1988) *Biochim. Biophys. Acta 934*, 314−328.
18. McPherson, P. H., Okamura, M. Y., and Feher, G. (1988) *Biochim. Biophys. Acta 934*, 348−368.
19. Hienerwadel, R., Thibodeau, D., Lenz, F., Nabedryk, E., Breton, J., Kreutz, W., and Mantele, W. (1992) *Biochemistry 31*, 5799−5808.
20. Hienerwadel, R., Grzybek, S., Fogel, C., Kreutz, W., Okamura, M. Y., Paddock, M. L., and Breton, J. (1995) *Biochemistry 34*, 2832−2843.
21. Nabedryk, E., Brenton, J., Hienderwadel, R., Fogel, C., Mantele, W., Paddock, M. L., and Okamura, M. Y. (1995) *Biochemistry 34*, 14722−14732.
22. Patel, K. B., and Willson, R. L. (1973) *J. Chem. Soc., Faraday Trans. 1 69*, 814−825.
23. Swallow, A. J. (1982) in *Function of Quinones in Energy Conserving Systems* (Trumpower, B. L., Ed.) pp 59−72, Academic Press, New York.
24. Shopes, R. J., and Wraight, C. A. (1985) *Biochim. Biophys. Acta 806*, 348−356.
25. Takahashi, E., Wells, T. A., and Wraight, C. A. (1998) in *Proceedings of the XIth International Photosynthesis Congress* (Garab, G., Ed.) pp 17−22, Kluwer Academic Publishers, Dordrecht, The Netherlands.
26. Takahashi, E., Warncke, K., and Wraight, C. A. (1998) *Biophys. J. 74*, A41.
27. Clayton, R. K., and Wang, R. T. (1971) *Methods Enzymol. 23*, 696−704.
28. Okamura, M. Y., Isaacson, R. A., and Feher, G. (1975) *Proc. Natl. Acad. Sci. U.S.A. 72*, 3492−3496.
29. Woodbury, N. W., Parson, W. W., Gunner, M. R., Prince, R. C., and Dutton, P. L. (1986) *Biochim. Biophys. Acta 851*, 6−22.
30. McComb, J. C., Stein, R. R., and Wraight, C. A. (1990) *Biochim. Biophys. Acta 1015*, 156−171.
31. Gunner, M. R., Tiede, D. M., Prince, R. C., and Dutton, P. L. (1982) in *Function of Quinones in Energy Conserving Systems* (Trumpower, B. L., Ed.) pp 265−269, Academic Press, New York.
32. Warncke, K., Gunner, M. R., Braun, B. S., Gu, L., Yu, C., Bruce, J. M., and Dutton, P. L. (1994) *Biochemistry 33*, 7830−7841.
33. Giangiacomo, K. M., and Dutton, P. L. (1989) *Proc. Natl. Acad. Sci. U.S.A. 86*, 2658−2662.
34. Takahashi, E., Maroti, P., and Wraight, C. A. (1992) in *Electron and Proton Transfer in Chemistry and Biology* (Müller, A., Ed.) pp 219−236, Elsevier, New York.
35. Takahashi, E., and Wraight, C. A. (1992) *Biochemistry 31*, 855−866.
36. Mathis, P., Sinning, I., and Michel, H. (1992) *Biochim. Biophys. Acta 1098*, 151−158.
37. Leibl, W., and Breton, J. (1991) *Biochemistry 30*, 9634−9642.
38. Moser, C. C., Keske, J. M., Warncke, K., Farid, R., and Dutton, P. L. (1992) *Nature 355*, 796−802.
39. Gray, H. B., and Winkler, J. R. (1996) *Annu. Rev. Biochem. 65*, 537−561.
40. Gopher, A., Blatt, Y., Schonfeld, M., Okamura, M. Y., Feher, G., and Montal, M. (1985) *Biophys. J. 48*, 311−320.
41. Franzen, S., and Boxer, S. G. (1993) *J. Phys. Chem. 97*, 6304−6318.
42. Marcus, R. A., and Sutin, N. (1985) *Biochim. Biophys. Acta 811*, 265−322.
43. DeVault, D. (1980) *Q. Rev. Biophys. 13*, 387−564.
44. Calvo, R., Passeggi, M. C., Isaacson, R. A., Okamura, M. Y., and Feher, G. (1990) *Biophys. J. 58*, 149−65.
45. Gunner, M. R., and Dutton, P. L. (1989) *J. Am. Chem. Soc. 111*, 3400−3412.
46. Ortega, J. M., Mathis, P., Williams, J. C., and Allen, J. P. (1996) *Biochemistry 35*, 3354−3361.
47. Lin, X., Murchison, H. A., Nagarajan, V., Parson, W. W., Allen, J. P., and Williams, J. C. (1994) *Proc. Natl. Acad. Sci. U.S.A. 91*, 10265−10269.
48. Dutton, P. L., and Moser, C. C. (1994) *Proc. Natl. Acad. Sci. U.S.A. 91*, 10247−10250.
49. Allen, J. P., Williams, J. C., Graige, M., Paddock, M. L., Labahn, A., Feher, G., and Okamura, M. Y. (1998) *Photosynth. Res. 55*, 227−233.
50. Dutton, P. L., Leigh, J. S., and Wraight, C. A. (1973) *FEBS Lett. 36*, 169−173.
51. Prince, R., and Dutton, P. L. (1976) *Arch. Biochem. Biophys. 172*, 329−334.
52. Gunner, M. R., Robertson, D. E., and Dutton, P. L. (1986) *J. Phys. Chem. 90*, 3783−3795.
53. Stowell, M. H. B., McPhillips, T. M., Rees, D. C., Soltis, S. M., Abresch, E., and Feher, G. (1997) *Science 276*, 812−816.
54. Alexov, E., and Gunner, M. (1999) *Biochemistry 38*, 8253−8270.
55. Grafton, A. K., and Wheeler, R. A. (1999) *J. Phys. Chem. 103*, 5380−5387.
56. Sebban, P. (1988) *Biochim. Biophys. Acta 936*, 124−132.
57. Sebban, P., and Wraight, C. A. (1989) *Biochim. Biophys. Acta 974*, 54−65.
58. Kalman, L., and Maroti, P. (1994) *Biochemistry 33*, 9237−9244.
59. Kalman, L., and Maroti, P. (1997) *Biochemistry 36*, 15269−15276.
60. Page, C. C., Moser, C. C., Chen, X., and Dutton, P. L. (1999) *Nature 402*, 47−52.

BI992591F